polymers

MDPI

Article

Research on the Physical Properties and Internal Structure of PVP/Nb_2O_5 Nanocomposite Coatings

Paweł Jarka [1,*], Pallavi Kumari [2], Małgorzata Łazarska [3], Marcin Godzierz [2], Sonia Kotowicz [4], Marek Marcisz [5], Marcelina Bochenek [2], Łucja Hajduk [5], Magdalena M. Szindler [1] and Barbara Hajduk [2,*]

[1] Department of Engineering Materials and Biomaterials, Silesian University of Technology, 18a Konarskiego Str., 41-100 Gliwice, Poland; magdalena.szindler@polsl.pl
[2] Centre of Polymer and Carbon Materials, Polish Academy of Sciences, 34 Marie Curie-Skłodowska Str., 41-819 Zabrze, Poland; pkumari@cmpw-pan.pl (P.K.); mgodzierz@cmpw-pan.pl (M.G.); mbochenek@cmpw-pan.pl (M.B.)
[3] Faculty of Materials Engineering, Kazimierz Wielki University, 30 Chodkiewicza Street, 85-064 Bydgoszcz, Poland; lazarska@ukw.edu.pl
[4] Institute of Chemistry, University of Silesia, 9 Szkolna Str., 40-006 Katowice, Poland; sonia.kotowicz@us.edu.pl
[5] Faculty of Transport and Aviation Engineering, Silesian University of Technology, 8 Krasińskiego Str., 40-019 Katowice, Poland; marek.marcisz@polsl.pl (M.M.); lh305756@student.polsl.pl (Ł.H.)
* Correspondence: pawel.jarka@polsl.pl (P.J.); bhajduk@cmpw-pan.pl (B.H.)

Abstract

The subject of this study is the effects of various concentrations of niobium pentoxide nanoparticles (Nb_2O_5 NPs) on the physical, optical, and thermal properties of thin films of poly(N-vinylpyrrolidone) (PVP). The obtained results indicate that the addition of nanoparticles significantly affects the physical properties of the investigated materials, limiting their optical UV transmittance in the range of 300–500 nm by approximately 20–40% and increasing the material's resistance to moisture that is present in the surrounding environment. Based on the thermal measurements performed using differential scanning calorimetry (DSC) and variable temperature spectroscopic ellipsometry (VASE), two distinct glass transition temperatures T_g for pure PVP and its Nb_2O_5 composites were revealed, with an additional intermediate T_g appearing in the composites, varying in the range of 135–168 °C (ellipsometric temperature cycle). This intermediate transition indicates the formation of an interfacial region with modified polymer chain mobility due to the interactions occurring between Nb_2O_5 nanoparticles and the PVP matrix. The results obtained from the scanning electron microscopy (SEM), Energy Dispersive Spectroscopy (EDS), and detailed Attenuated Total Reflectance-Fourier Transform Infrared Spectroscopy (ATR-FTIR) analyses also confirmed the presence of this interfacial area and indicated that it arises from nanoparticle agglomeration and surface cluster formation. The contact angle measurements revealed that the composites containing 15% and 25% Nb_2O_5 exhibited greater hydrophobicity. These results suggest that the investigated composite coatings could be employed as surface coverings to protect against external, environmental influences, such as moisture and UV radiation.

Keywords: PVP-Nb_2O_5 composites; thin films; physical properties; variable temperature spectroscopic ellipsometry

check for updates

Academic Editor: Andrea Sorrentino

Received: 22 September 2025
Revised: 30 October 2025
Accepted: 1 November 2025
Published: 3 November 2025

Citation: Jarka, P.; Kumari, P.; Łazarska, M.; Godzierz, M.; Kotowicz, S.; Marcisz, M.; Bochenek, M.; Hajduk, Ł.; Szindler, M.M.; Hajduk, B. Research on the Physical Properties and Internal Structure of PVP/Nb_2O_5 Nanocomposite Coatings. *Polymers* **2025**, *17*, 2939. https://doi.org/10.3390/polym17212939

Copyright: © 2025 by the authors. Licensee MDPI, Basel, Switzerland. This article is an open access article distributed under the terms and conditions of the Creative Commons Attribution (CC BY) license (https://creativecommons.org/licenses/by/4.0/).

1. Introduction

Nanocomposites, in the form of polymer matrices that incorporate organic or inorganic nanoadditives that are uniformly distributed on the nanoscale 10–100 nm and are created

through physical mixing processes, present unique chemical and physical characteristics that improve material performance have attracted the attention of researchers around the world [1]. Modern composites reinforced with nanostructures exhibit significantly improved mechanical properties, chemical resistance, thermal stability, reduced permeability, flame resistance, electrical conductivity, and optical performance [2]. The nanofillers used can be, depending on the application, particles, fibers, or even agglomerates embedded in a variety of natural or synthetic polymers. Hence, these materials have great potential for use, especially in aeronautics, automotive, and electronics, as well as in medicine, due to their exceptional qualities [3].

From a production and application perspective, polymer nanocomposites (PNCs) take advantage of the lightweight, flexible nature of polymers, as well as the simplicity of their production and shaping, through cost-effective processes. The PNC materials can be modified depending on the nanoadditive particle's shape, size, specific surface area, and chemical nature. The selection of nanofiller properties, as well as their homogeneous distribution within the PNC structure, generates phase compatibility, which determines their applicability in various technologies [4,5]. The analysis of scientific literature leads to the conclusion that, depending on the conditions of their synthesis and surface chemistry, the nanoparticles show a strong tendency to form agglomerates. These agglomerates can be classified as hard agglomerates (created by smaller particles connected by sinter necks) and soft agglomerates (created by accumulations of particles connected by attractive physical interactions like van der Waals or hydrogen bridges). The formation of agglomerates is determined by the interactions between nanofiller particles, i.e., their surface chemistry, particle shape, aspect ratio, dimensionality, interparticle distance, and polydispersity [6]. The hard agglomerates can be crushed by high-energy milling, while soft agglomerates are dispersed by shear forces, generating gradients of the mechanical stress.

A particularly interesting application of PNCs is the combination of the functional properties of the matrix polymer and the specific properties of the nanofiller in the structure of a protective coating. The simplicity and cost-effectiveness of producing PNC coatings make them ideal materials for, e.g., UV-blocking applications. Generally, UV light protection coatings are created by incorporating UV-blocking inhibitors or light protection components [5,7]. Currently, UV blockers are used in the form of inorganic fillers, such as metal oxides like TiO_2, ZnO, SiO_2, CeO_2, and Fe_2O_3, minerals like $CaCO_3$ clays, semiconductors like CdSe, CdS, CdTe, and PbS, and metals and their alloys like Ag, Cu, Au, Fe, and Ge, which are dispersed in polymer matrices [8]. In particular, nanostructured fillers, which achieve a maximum absorption in the UV region (200–400 nm), are capable of efficiently absorbing UV radiation [8,9]. The challenge, however, is to combine the unique optical properties, chemical stability, environmentally friendly nature, and low cost of the inorganic fillers [10] in combination with organic molecules of the matrix. The physical properties of the nanoadditives and their proper distribution within the matrix are crucial for their potential applications [11]. Due to the physical, mechanical, chemical, and thermal properties, polyvinyl alcohol (PVA) [12,13] and polyvinyl pyrrolidone (PVP) are considered to be the matrix for UV protective films. Amorphous PVP is a biocompatible material with high environmental stability [13,14]. However, PVP tends to oxidize when exposed to UV radiation [15–17].

It should also be noted that the thermal stability of PNCs in low-cost, large-area protective structures is essential. In polymer film fabrication, scientists aim to increase the crystallinity of films by controlling the evaporation rate or by using external physical force [18–23]. The application of external stress (shear, centrifugal force, or capillary forces) contributes to the formation of directional structures in spin-coating, drop-casting, bar-coating, or solution-shear processes.

To date, there has been no detailed study on the effect of one of the most promising metal oxide semiconductors, Nb_2O_5, on the photoelectric properties (such as the high refractive index, wide bandgap, good optical quality, and negligible scattering), chemical stability, and thermal stability of PVP/NP structures [16,17].

An extremely important application aspect for polymer-based composite films, especially in applications as protective films, is the determination of their surface wettability, which provides information about surface energy and interactions with liquids. Many well-researched and traditionally used polymers, despite their excellent performance properties, such as their low weight, transparency, and processability, are limited in their use as protective films due to their hydrophilic nature [24]. In such cases, structural modifications of polymers or their combination with hydrophobic polymers are used, e.g., when modifying membranes, which allows obtaining specific surface properties, including hydrophobicity. In the work of Jebali et al., a two-step process was used to obtain hydrophobic PVP films [25]. In the cited work, crosslinking with benzophenone and UV irradiation was used, which led to the formation of water-insoluble PVP, and additionally, the surface of the film was modified by the addition of silica nanoparticles. The related investigation of the hydrophobic properties of polymer/NP coatings was provided by Yousef et al. [26]. The authors modified the PVC/PVP composites using $BiVO_4$ nanoparticles, where the addition of these NPs led to a decrease in the water contact angle.

The novelty of this article lies in the use of a unique combination of an organic polymer PVP matrix and inorganic semiconductor nanoparticles Nb_2O_5, which allows for the production of coatings with relatively hydrophobic properties that can also protect the coated surface from UV radiation. Such coatings can be relatively easily applied to larger areas, such as parts of various mechanical devices that are exposed to environmental factors. This, in turn, provides a relatively wide range of potential applications, for example, in the automotive, aviation, and medical industries.

2. Experimental Section

2.1. Materials and Samples Preparation

The materials that we used are poly(N-vinylpyrrolidone) (PVP) [27,28] with a molecular weight of 40,000 g/mol, and niobium pentoxide Nb_2O_5, with a diameter of around 70 nm (purity 99.9%) [29,30]. PVP and Nb_2O_5 were supplied by Sigma-Aldrich. The chemical structures of these materials are presented in Figure 1a,b.

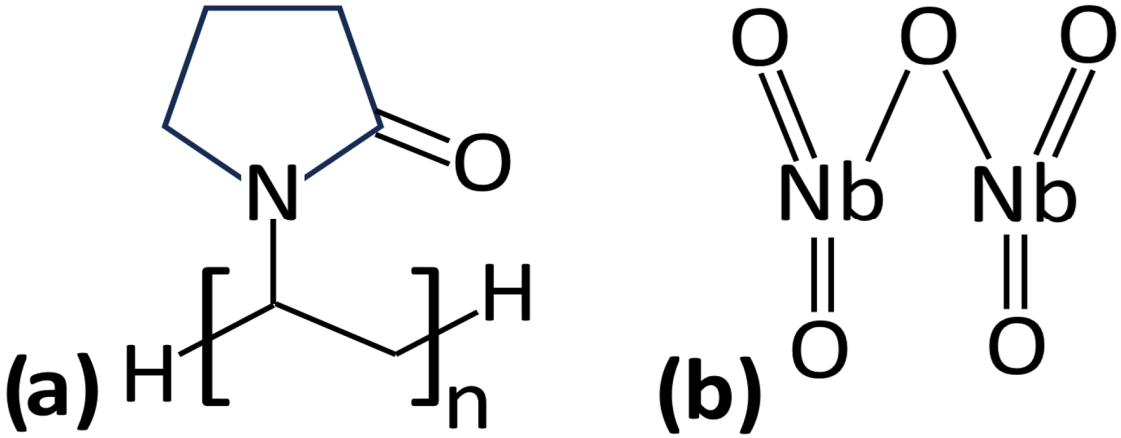


Figure 1. Chemical structures of PVP (**a**) and Nb_2O_5 (**b**).

Thin films of PVP and its composites were obtained from a chloroform solution. The weight concentration of each sample solution was constant, i.e., 20 mg/mL. For each

sample, 1 mL of a polymer-NP solution was prepared (which ensured the preparation of approximately four films). In Table 1, the percentage indicates the weight fraction of the Nb_2O_5 nanoparticles in a 20 mg/mL solution; for example, in samples containing 10% by weight of NPs, 2 mg of Nb_2O_5 was used compared to 18 mg of PVP, which constituted the remaining 90%.

Table 1. Percentage content and weight of individual chloroform/polymer/NP solutions.

Polymer content (%)	100	90	85	75	65
NPs content (%)	0	10	15	25	35
PVP weight (mg)	20	18	17	15	13
Nb_2O_5 Weight (mg)	0	2	3	5	7

Prior to applying the thin films using the spin-coating technique, the solutions were homogenized using the pulse mode with an energy input of 15.1 kJ, power of 20 W, and a pulse time of 11 s for 10 min using a Bandelin Sonopuls homogenizer. The films were coated directly from homogenized solutions with the spinning time t = 60 s, and the spin speed V = 1200 rpm, with the acceleration time t = 2 s.

2.2. Methods

To perform the ellipsometric studies, we used the SENTECH SE850E spectroscopic ellipsometer, which was operated by the Spectra Ray 3 software, working within the spectral range of 240 to 2500 nm. Three ellipsometric modes were applied: the transmission mode (using a specific sample holder), the variable angle mode (using a standard automated table), and the variable temperature mode (using a temperature-controlled cell, INSTEC mK1000, operating under decreased pressure). Transmission mode measurements were performed across the whole UV–Vis/NIR spectrum. For incidence angles between 40° and 70°, ellipsometric angles Ψ and Δ were recorded in 5° increments. The protocol described in our earlier studies was followed in the variable temperature experiments [31–34]. Each sample was heated separately to 250 °C for 5 min while being kept under the pressure of 10^{-3} Torr. The films were then quickly cooled to −100 °C within three minutes. Every temperature cycle was conducted at a heating rate of 2 °C/min. The temperature controller and a liquid nitrogen pump were used to control the temperature of the table (and at the same time, the temperature of the sample).

The transmission mode of the ellipsometer was used for the optical transmission measurements, and the variable angle spectroscopic ellipsometry (VASE) was used for film and roughness thickness measurements and for determining the refractive indices. Using the VTSE, we have determined the thermal transition temperatures.

The DSC analysis was performed on TA DSC 25 Discovery instruments with a heating and cooling rate of 20 °C/min in a constant stream of nitrogen (20 mL/min) atmosphere to 250 °C in the aluminum pans.

SEM imaging, elemental compositional analysis (EDS analysis), and surface roughness measurements were taken using a Phenom XL microscope (Thermo Fisher Scientific) with backscattered electron detection (BSD) that was equipped with an energy-dispersive X-ray spectroscopy (EDS) detector and 3D surface reconstruction module (Phenom 3D). The analysis was conducted at accelerating voltages of 5 kV and 10 kV, after sputter-coating the sample with a gold film to improve surface conductivity.

Contact angle measurements were performed at room temperature by applying a drop of distilled water (with a volume of V = 2–4 μL) onto the test surface using a glass syringe. The contact angle measurement results are the arithmetic mean calculated from 30 images

taken at 1 image/sec. Measurements were performed using a CAM101 goniometer (KSV Instruments) equipped with a camera (resolution 640 × 480 pixels) and an external temperature adapter (Intelligent Digital Controller OMRON5EGN). CAM2008 software was used for data analysis and calculations.

X-ray diffraction (XRD) scans were performed on polymer and composite films deposited on cover microscopic glass substrates using a D8 Advance diffractometer (Bruker, Karlsruhe, Germany) with a Cu-Kα cathode (λ = 1.54 Å) in the coupled Two-Theta/Theta mode. The scan rate was 1.2°/min, with a step size of 0.02° in the 2θ range of 2° to 60° (dwell time 1 s). The analysis was performed with DIFFRAC.EVA software V5.1.

ATR-FTIR measurements were provided with a Nicolet 6700 Thermo Fisher device, which worked in the range of 2.5–25 μm.

3. Results and Discussion

3.1. XRD Analysis

The X-ray diffraction (XRD) patterns of the PVP and its Nb_2O_5 composite films, with 5, 15, 25, and 35% NPs concentrations, deposited onto microscopic cover glass substrates, are presented in Figure 2.

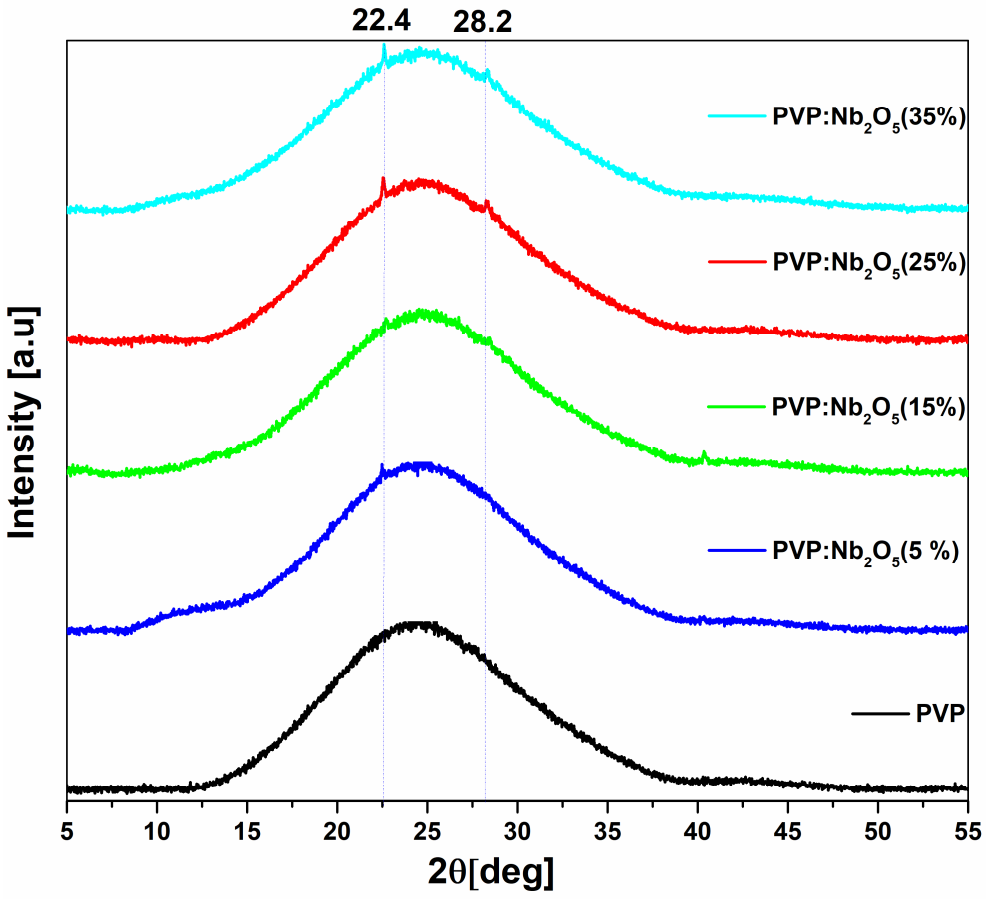


Figure 2. XRD patterns of PVP (black line) and its Nb_2O_5 composites (color lines).

For reference, the XRD pattern of pure Nb_2O_5 nanoparticle powder has been added to the Supplementary Materials (see Figure S1a). There are two visible strong peaks, located at 2θ = 22.4 and 28.2 deg, which are characteristic of this material.

The diffraction spectrum of the pure polyvinylpyrrolidone (PVP) film exhibits a broad, featureless hump, which is characteristic of its amorphous nature. In the case of the sample with a 5% NPs content, we observed one weak peak at 2θ = 22.4°, coming from

Nb_2O_5, which is related to the low NPs content and formation of sparse NPs clusters. In contrast, the remaining XRD patterns of the composite films, prepared with Nb_2O_5, in concentrations of 15, 25, and 35%, displayed two distinct diffraction peaks: −22.4 and 28.2° (the second one also originates from NPs). At the 15% concentration, more agglomerated clusters appear—likely smaller in size. However, due to their higher number, a second peak appeared compared to the 5% sample. This result partially indicates a relatively uniform distribution of nanoparticles in the PVP matrix. At the higher concentrations (25% and 35%), the diffraction peaks become slightly more pronounced, indicating that the Nb_2O_5 concentration in these samples is higher and that a larger number of agglomerates have likely formed, possibly with a greater diameter. The XRD pattern of PVP: Nb_2O_5 (35%) with a subtracted amorphous hump, with marked Nb_2O_5, has been added to the Supplementary Materials (Figure S1b).

3.2. Ellipsometric Analysis

The transmission spectra of the pure PVP films and their composites with Nb_2O_5 nanoparticles, deposited on a microscopic coverglass, are presented in Figure 3. These measurements were performed using the transmission mode of the ellipsometer. The range of obtained spectra was limited to 2000 nm due to the large spectra fluctuations in the range of 2000–2500 nm.

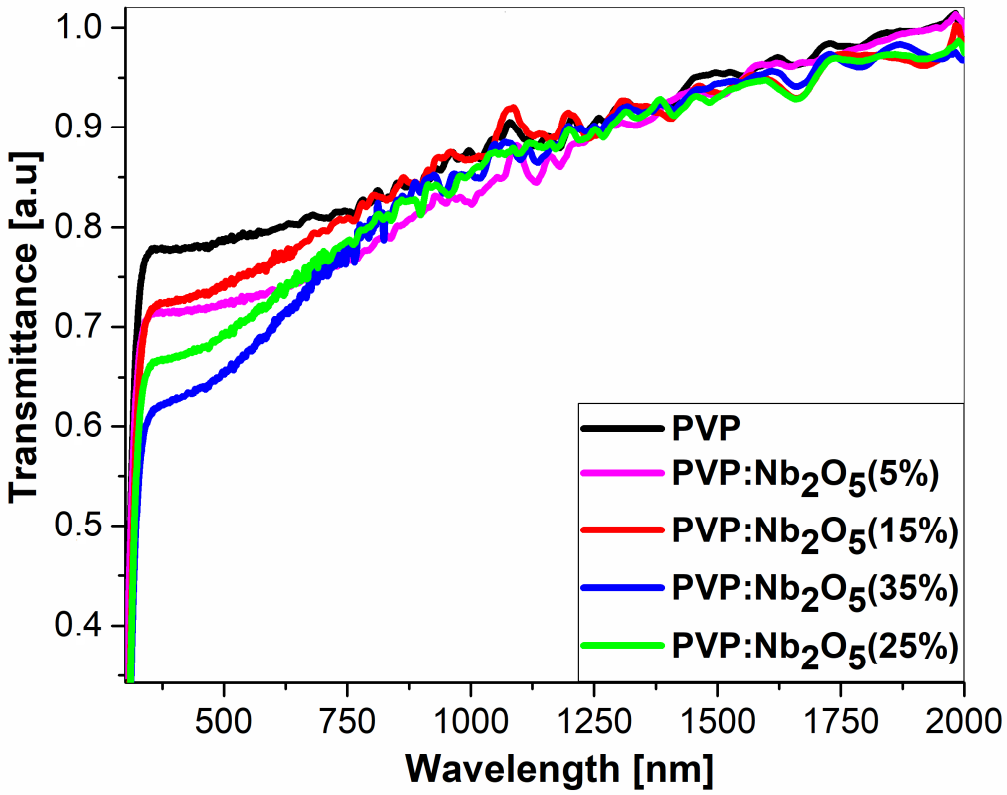


Figure 3. Transmittance of PVP and its Nb_2O_5 composites.

All the curves were normalized at a wavelength of λ = 2000 nm to account for the differences in the thicknesses of the prepared films (see Table 2). The spectra within the full range and that are non-normalized can be found in Supplementary Materials (see Figure S2).

It can be seen that the spectrum of the pure polymer PVP film is highly transparent, providing light transmission of at least 80% across the entire measured range. In the case of the composite spectra, a significant decrease in the light transmission in the UV–visible range (320–700 nm) can be observed, with the strongest reduction occurring

between λ = 320 to 500 nm. These results may be important for potential applications of the investigated materials.

Table 2. Physical parameters of PVP and its composites.

Thin Film	PVP	PVP: Nb_2O_5 (5%)	PVP: Nb_2O_5 (15%)	PVP: Nb_2O_5 (25%)	PVP: Nb_2O_5 (35%)
Refractive index *n* [a.u] (for λ = 2500 nm)	1.521	1.522	1.525	1.528	1.531
Fraction coefficient f [a.u]	0	0.004	0.010	0.017	0.024
Thickness of films on SiO_2 d [nm]	303	371	255	466	208
Roughness of films on SiO_2 r [nm]	146	134	128	162	160
Thickness of films on micr. cover glass d [nm]	257	302	270	285	340
Roughness of films on micr. cover glass r [nm]	101	120	97	115	134

Variable angle spectroscopic ellipsometry (VASE) was used to determine the refractive index dispersion of the prepared samples. Measurements in the 240–2500 nm wavelength range were performed on PVP polymer films and their Nb_2O_5 composites, which were deposited onto silicon substrates coated with 300 nm of SiO_2. The ellipsometric model, which was used for fitting the theoretical curve to the obtained experimental data (for the Ψ and Δ ellipsometric angles and the degree of polarization), consisted of five component layers: air, a roughness layer, a polymer/composite layer, and two substrate layers, as is presented in Figure 4. A roughness layer was modeled using the effective medium approximation model (EMA), combining the composite layer and the air layer, where air was treated as a non-dispersive medium. The polymer/composite layer was modeled using a Cauchy model for the pure polymer [35–37], while the composite was modeled using an EMA-type model, fitted for PVP and a Cauchy model of Nb_2O_5 material layer, taken from the database of ellipsometric models that are available in SpectraRay 3 software. Finally, an air layer with a refractive index of 1 was included. The so-called volume fraction coefficient was used to determine the Nb_2O_5 nanoparticles content in the PVP matrix. This coefficient corresponds to the volume fraction of nanoparticles relative to the volume of polymer and is not identical to the weight percentage ratio of nanoparticles to polymer. The formula for the volume fraction coefficient f is given in Equation (1), and the obtained values are presented in Table 2.

The Bruggeman formula yielded the volume fraction coefficient [38] that was used for a polymer or composite layer:

$$f\frac{\varepsilon_i - \varepsilon_{eff}}{\varepsilon_i + 2\varepsilon_{eff}} + (1 - f)\frac{\varepsilon_m - \varepsilon_{eff}}{\varepsilon_m + 2\varepsilon_{eff}} = 0 \quad (1)$$

where f is the volume fraction coefficient of nanoparticles, ε_i is the nanoparticles' dielectric coefficient (inclusion material), ε_m is the polymer dielectric coefficient (host material), and

ε_{ff} is an effective dielectric coefficient of the investigated material (composite). Based on this formula, it was possible to derive the dependence relation on the coefficient of volumetric fraction:

$$f \approx \frac{\varepsilon_{eff} - \varepsilon_m}{3\varepsilon_m} \cdot \frac{\varepsilon_i + 2\varepsilon_m}{\varepsilon_i - \varepsilon_m} \quad (2)$$

The obtained volume fraction coefficient values, along with the film thickness, surface roughness, and refractive index for the wavelength λ = 2000 nm, are shown in Table 2. Also, the dispersions of refractive indices, generated for PVP, Nb_2O_5 (Sentech ellipsometric database), and for composites with different Nb_2O_5 percentage contents that were deposited onto silicon substrates, are presented in Figure 5. It is noticeable that the dispersions are presented in the range of 500 to 2500 nm. The reason for this approach is the degree of light polarization in the 240–500 nm region, the deviation of which significantly exceeds 10%. Additionally, the number of spectra used in the theoretical fit was limited to incidence angles of 40–50°, because for angles of 60–70°, the degree of polarization significantly deviated from 1 over the entire measured wavelength range. The refractive index n of pure PVP is around 1.521, while that n of Nb_2O_5 is approximately 2.097. With respect to the weight percentage of the nanoparticles, the n value for Nb_2O_5 should significantly affect the refractive index of the composite. However, ellipsometric fits indicate otherwise. The n values for the individual NPs percentages—5%, 15%, 25%, and 35%—are 1.522, 1.525, 1.528, and 1.531, respectively, and thus do not differ significantly from the refractive index of the polymer matrix. This is due to the low values of the volume fraction coefficients, which for the composites are f = 0.004, 0.010, 0.017, and 0.024, respectively. Note that f is the factor that is determined from the optical model with the best possible fit (for the lowest mean square error (MSE) value obtained). Being dimensionless, the volume factor differs from the weight factor. Because the f values are low, this means that only a small percentage of nanoparticles contained in the polymer matrix have an active influence on the composite's refractive index. Another reason for such low f values may be the relatively high surface roughness, which is reflected in the determined surface roughness coefficient values (see Table 2). The obtained ellipsometric results are in very good agreement with the SEM surface roughness analysis (see Supplementary Materials, Figure S2).

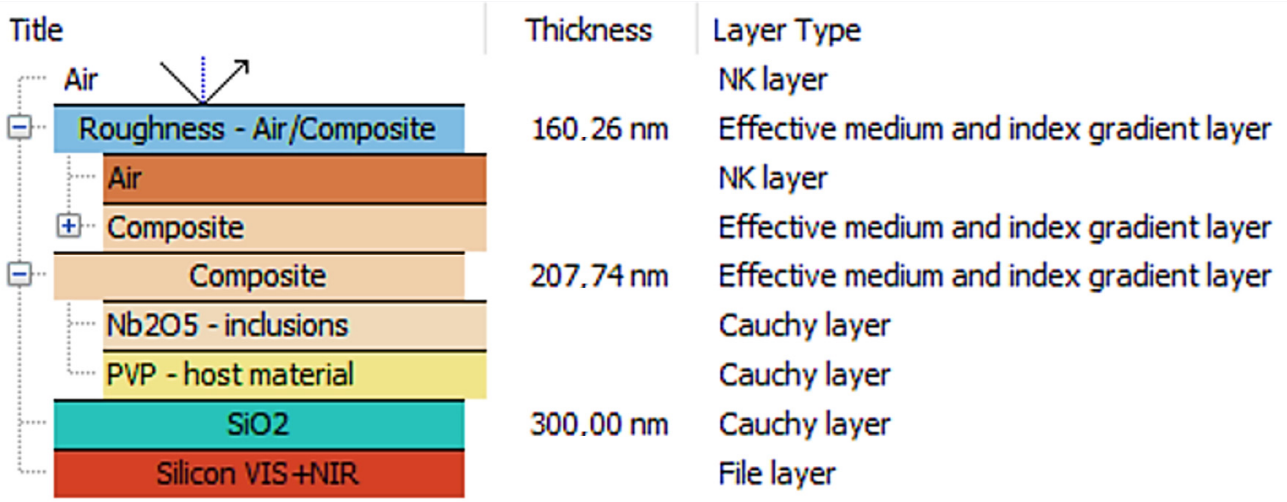


Figure 4. The ellipsometric model used for PVP and its NPs composite spectra fitting.

Based on the obtained results, we can assume that the nanoparticles contained in the polymer form agglomerates that cause light scattering in the 300–500 nm range. However, this has no significant effect on light transmittance in the remaining spectral range, where the wavelength is longer, and, therefore, the nanoparticle agglomerates become

"invisible to the beam." The low refractive index values measured at a wavelength of 2000 nm also confirm this fact. The formation of agglomerates is confirmed by the results obtained using SEM microscopy and may also affect the thermal properties of the resulting composite films.

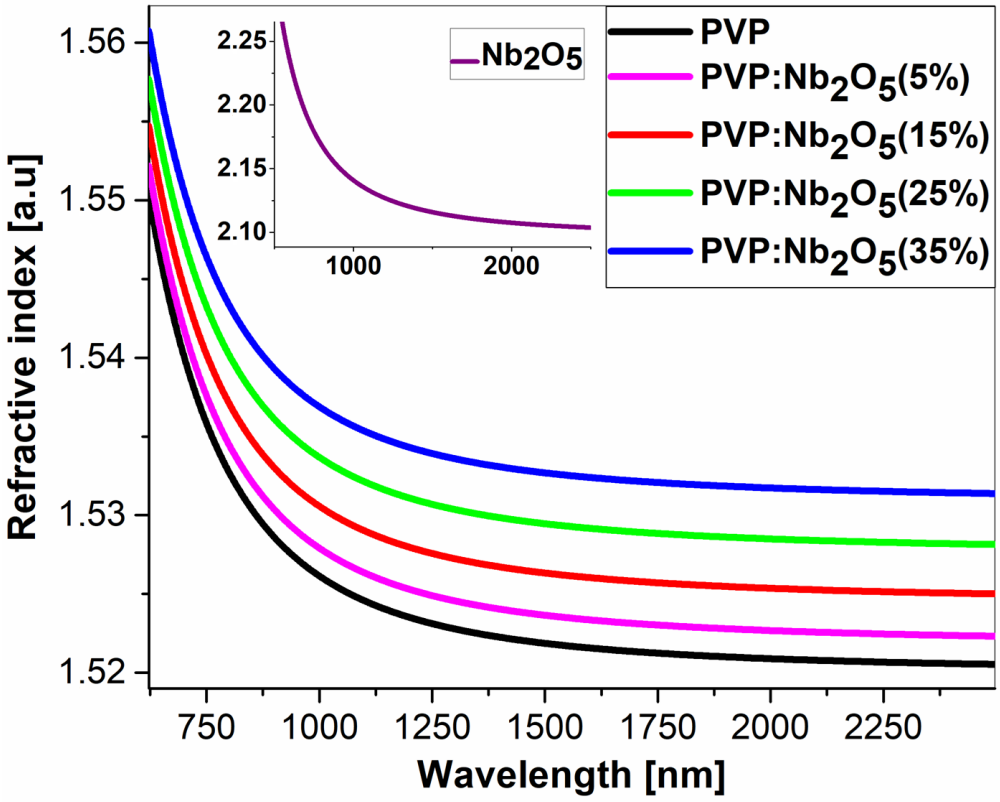


Figure 5. Values of refractive indices of PVP and its composites with Nb_2O_5. The refractive index of Nb_2O_5 has been added as the inset for comparison.

3.3. Thermal Analysis

The thermal analyses of pure PVP and its composites were performed using two methods: DSC and VTSE, and the obtained results were then compared. The DSC analysis included measurements of the starting materials in powder form after solvent evaporation. The obtained DSC plots for the PVP and composites are presented in Figure 6, and the individual, detected thermal transition temperatures are shown in Table 3. The results indicate the presence of two glass transition temperatures (T_g). For both pure PVP and its composites, the first temperature (T_{g1}) is equal to 88–89 °C and is, therefore, practically constant. All of the results also indicate a second glass transition temperature (T_{g2}), with values detected for pure PVP and its composites with Nb_2O_5 (5, 15, 25, and 35%) of 188, 181, 180, 183, and 204 °C, respectively. The typical T_g temperature of PVP is included within the temperature range of 150–180 °C [39–42]. In the case of the plot, obtained for the pure material, we have recorded the temperatures of 88 and 188 °C. Two explanations for the obtained results are possible. The first approach suggests that T_{g1} = 88 °C is a temperature derived from secondary β-segmental relaxation, which was very well described by Vyazovkin and Dranc [43]. The pyrrolidone ring's rocking motions as it rotates around the C-N bond are the cause of this phenomenon, which is independent of the molecular weight. Compared to the glass transition energy of the polymer backbone, this type of motion has a lower energy barrier.

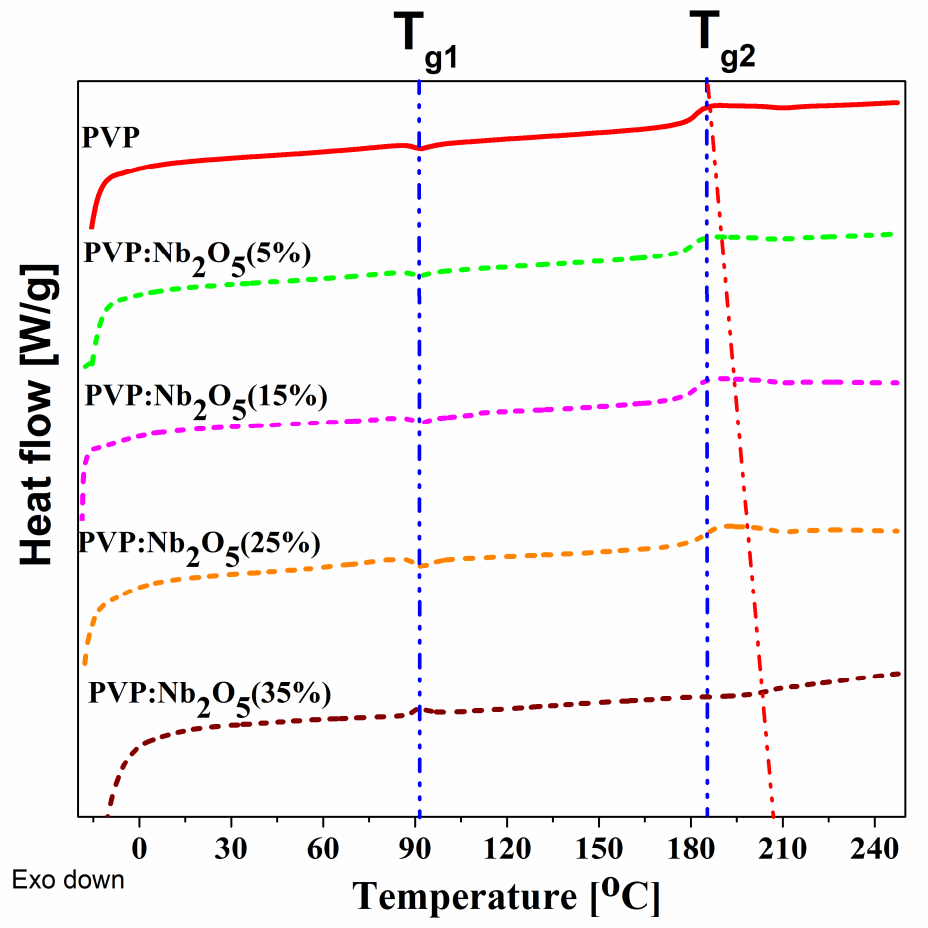


Figure 6. The DSC plots, obtained with a heating rate of 20 °C/min for pure PVP and its Nb_2O_5 composites (5, 15, 25, and 35%). The red line represents the T_g deviation for the highest nanoparticle concentration compared to pure PVP.

Table 3. Thermal properties: Glass transition temperature of polyvinylpyrrolidone and its composites with Nb_2O_5 using DSC and VTSE.

	DSC (Powder)		Temperature Ellipsometry (Films)		
Sample	**T_{g1} (°C)**	**T_{g2} (°C)**	**T_{gV1} (°C)**	**T_{gV2} (°C)**	**T_{gV3} (°C)**
PVP	88	188	92	-	197
PVP: Nb_2O_5 (5%)	88	181	104	142	204
PVP: Nb_2O_5 (15%)	88	180	105	168	198
PVP: Nb_2O_5 (25%)	89	183	95	151	207
PVP: Nb_2O_5 (35%)	88	204	91	135	202

The second possible explanation is the presence of a PVP fraction with a very low molar mass, which could indicate that the investigated material is a mixture of two molecular weight fractions (40,000 g/mol and a much lower one). Using the Flory–Fox relation (Equation (3)) for the amorphous polymers [44], the molar mass of the second fraction can be determined to be approximately 3000 g/mol. The Flory–Fox relation is described with the following well known equation:

$$T_g = T_{g\infty} - \frac{C}{M} \quad (3)$$

where $T_{g\infty}$ is the glass transition of the polymer with a high molecular mass (in our case, it is around 180 °C), M is the average molecular mass, and C is a constant characteristic of the individual polymer. In the case of the second T_{g2} temperature, the largest shift is observed for the highest nanoparticle concentration. Since this T_{g2} value is typical for PVP, the changes in its value can be explained by the presence of nanoparticles. Nb_2O_5 nanoparticles, present in the polymer matrix, reduce the vibrations of the polymer backbone, stiffening it. This interaction increases the energy barrier, beyond which the glass transitions can occur.

Referring to our previous studies of thermal transitions of composite films [45,46] using variable temperature spectroscopic ellipsometry, it should be noted that it is quite convenient and quick to use raw ellipsometric data for a selected wavelength [47–49]. In this paper, we present thermal studies that were conducted using differential scanning calorimetry methods and compare them with the results obtained using the VTSE method. Here, we have selected the Ψ angle at a wavelength of λ = 900 nm. The restricted spectral range used for temperature monitoring and the high transmission in this range are the reasons for selecting this wavelength. The ellipsometric temperature cycles, recorded for films of PVP and its composites, deposited onto silicon substrates, are presented in Figure 7, and the obtained temperatures are presented in Table 3. For pure PVP, we have detected two temperature values: 92 and 197 °C, which correspond to the two T_g values obtained using the DSC method. This is typical, as the differences between the DSC and VTSE scans usually range from 10 to several degrees Celsius due to the different physical forms of the investigated materials (film in the case of VTSE; powder in the case of VTSE) [32]. Observations of the ellipsometric temperature scans led to very interesting conclusions. For the composites, whose content of Nb_2O_5 nanoparticles is equal to 5 and 15%, we noticed an increase in the first T_{gV1} value, from 92 °C (recorded for pure PVP film) to 104 and 105 °C, respectively. For the concentrations of 25 and 35%, the temperature values were shifted again to values closer to those for pure PVP: 95 and 91 °C, respectively. For T_{gV3}, which corresponds to the T_{g2} (the second glass transition temperature that is observed in DSC plot), we observed shifts in the temperature range of 198–207 °C. It can be easily noticed that, unlike the results obtained using the DSC method for the powdered material, each ellipsometric curve shows an intermediate temperature, which is absent in the case of the PVP matrix film without the addition of nanoparticles. The value of this intermediate temperature T_{gV2} changes varies significantly with the NP concentration, being the highest for a concentration of 15% Nb_2O_5, and the lowest for 35%. Changes in T_{gV1} and T_{gV3} can be easily explained by the stiffening of the PVP polymer chains. The most important temperature appears to be the T_{gV2} (Figure 7a), which can be related to the nanoparticles' agglomeration. Because spectroscopic ellipsometry is an extremely sensitive method for detecting changes in the physical parameters (e.g., the thickness), the effect must be linked to the interaction between the Nb_2O_5 NPs and the polymer. In the work of Ali et al. [50], it was shown that C=O···HO–Nb hydrogen bonds formed between Nb_2O_5 nanoparticles and the PVP/PVA polymer matrix, where C=O originates from the PVP pyrrolidone ring, the -OH group from PVA, and Nb-OH represents hydroxyl groups on the niobium pentoxide surface, which can act as donors or acceptors of hydrogen bonds. We believe that a similar problem occurs in our composite films. When nanoparticle concentrations are lower and more uniformly distributed in the polymer matrix, larger numbers of such linkages can be formed, resulting in a larger amount of this "third", intermediate phase. The glass transition temperature T_{gV2} appears as a consequence of the increased interfacial surface area, formed between the Nb_2O_5 nanoparticles and the PVP polymer, leading to the formation of a PVP phase with modified chain mobility (Figure 7b). At higher nanoparticle concentrations (25% and 35%), a large number of nanoparticle agglomerates

are present, causing the T_{gV2} temperature to be shifted to 151 °C and 135 °C, respectively. Fewer hydrogen bonds develop around larger agglomerates, which pushes the polymer chains apart (Figure 7c). Furthermore, the so-called dilution effect applies here: when the weight concentration of the solutions from which the films were derived remains constant, the sample contains less polymeric material and proportionally more nanoparticles than samples with lower concentrations. These two factors lead to a decrease in T_{gV2} at the highest Nb_2O_5 concentrations. It should be noted that T_{gV2} does not appear in the DSC results because the DSC results were presented for the same material in powder form. This temperature is related to the agglomeration of nanoparticles in the polymer matrix when an interface forms between PVP and Nb_2O_5 in layers where the material is continuous because it has been exposed to a solvent.

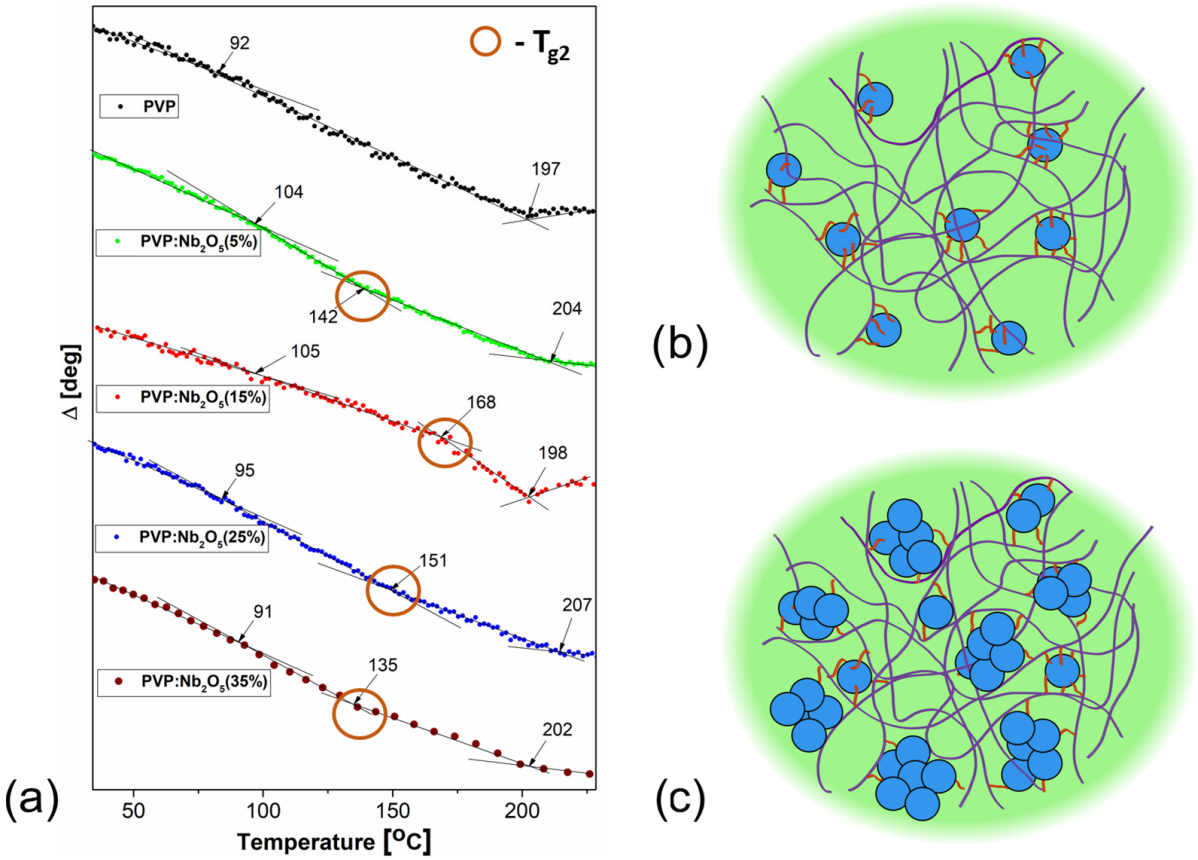


Figure 7. The ellipsometric angle Δ plot at 900 nm as a function of temperature for PVP and its Nb_2O_5 composites, (**a**) and nanoparticles distributed at lower (**b**) and higher concentrations (**c**).

3.4. ATR-FTIR Analysis

Unannealed films of PVP and its Nb_2O_5 composites, deposited on silicon substrates, underwent FTIR investigation. The clean substrate spectrum was subtracted from all spectra, and the baseline was applied to each of them. For clarity, Figure 8 displays the spectra within the 450–4000 cm^{-1} wavenumber range. The spectra of individual samples, highlighting the most significant peaks, are displayed in the Supplementary Materials in Figure S3a–e.

Peaks at frequencies of 734, 781, 1004, 1130, 1288, 1423, 1660, 2856, 2920, and 2954 cm^{-1} are present in the PVP spectrum. The PVP spectrum (Supplementary Materials Figure S3a) features peaks at frequencies of 734, 781, 1004, 1130, 1288, 1423, 1660, 2856, 2920, and 2954 cm^{-1}. Of these, 734 is a peak originating from C-H vibrations in the pyrrolidone ring, and 781 is a deformational C-H vibration. The peaks placed at about 1130 and 1288 cm^{-1} originate from C-N vibrations, where the first is the C-N stretching vibration,

associated with C-C stretching within the pyrrolidone ring, and the second one (1288) is a C–N stretching vibration in the N–C=O, characteristic for the pyrrolidone group. The 1423 and 1454 peaks are coming from CH2 scissor vibrations, 1660 from valence vibrations of the C=O group, and vibrations 2856, 2920, and 2954 originate from the C-H groups. The 2856 peak originates from asymmetric vibrations of C-H in CH_2 groups in the polymer chain, the 2920 is the asymmetric vibration of the same C-H bonds, and the 2952 peak is the asymmetric vibration of C-H in CH_3 in the pyrrolidone ring or in the polymer chain endings.

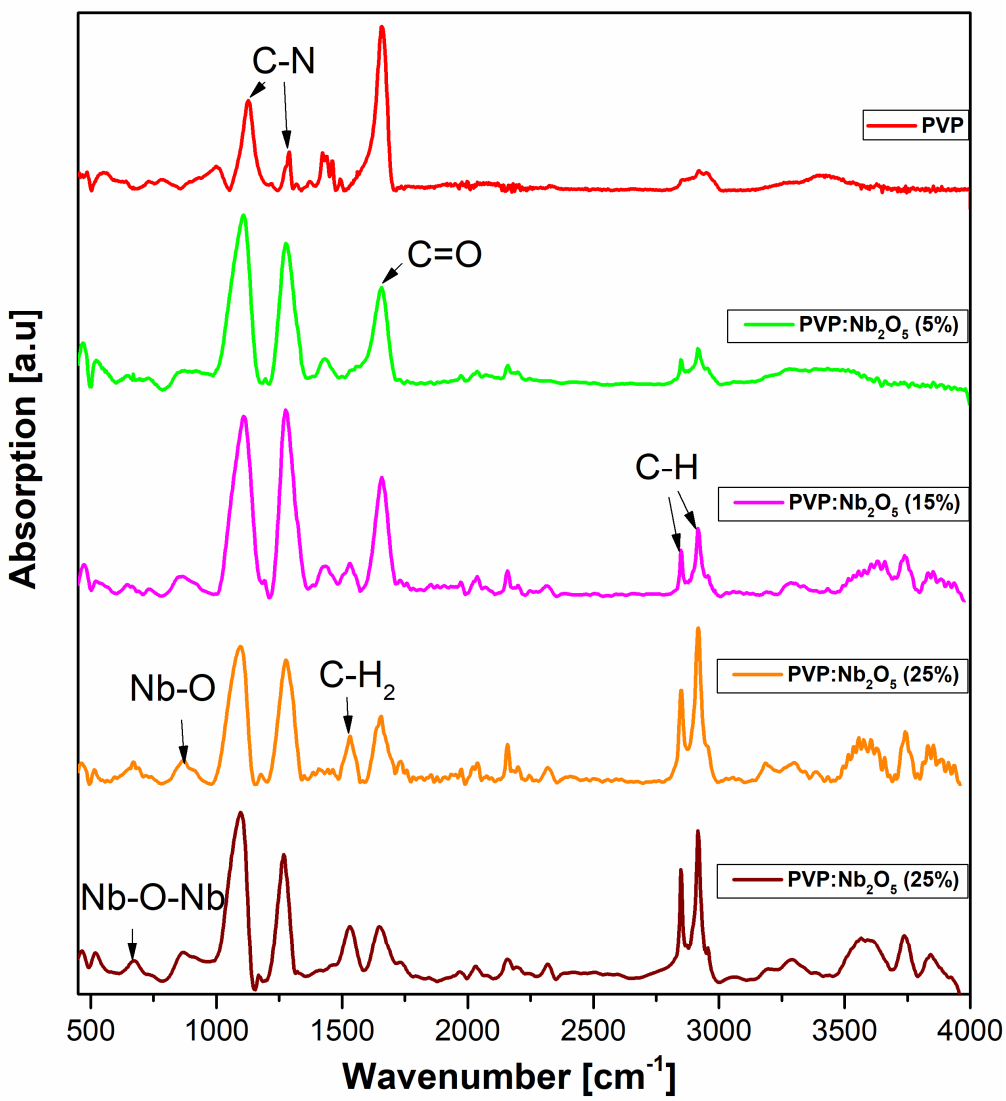


Figure 8. The ATR-FTIR spectra of PVP and its Nb_2O_5 composites.

In the spectrum of PVP with a 5% Nb_2O_5 content (Supplementary Materials Figure S3b), the peaks are located at wavenumber values of 645, 881, 1108, 1280, 1430, 1657, 2161, 2849, and 2913 cm^{-1}. Two new peaks can be observed, located at frequencies of 645 and 881 cm^{-1}. These peaks originate from the Nb-O-Nb bridge vibrations and the Nb-O stretching vibrations, respectively. The presence of Nb_2O_5 NPs was also fully confirmed by EDS analysis (see Supplementary Materials, Section S4). The additional peak appearing at the concentration of 15% of NPs at about 1538 cm^{-1} comes from coupled N–C=O/C–N vibrations in the pyrrolidone ring. The origination of individual peaks in the rest of the spectra, with the NPs concentration 15–35% (Supplementary Materials Figure S3c–e), is the same.

In the subsequent composite spectra, we can observe that the intensity of C-N peaks (1130 and 1288 cm^{-1}) is noticeably higher compared to the spectrum of pure PVP. It is the result of the interaction of pyrrolidone rings with Nb_2O_5, which influences the dipole moments of the C–N and N–C=O vibrations. We observed the highest intensity peak of 1288 for the PVP spectrum with 15% NPs.

The decreasing increase in the CH_2 peak's intensity (1438) at the concentrations 25 and 35%, and the appearance of the new one at 1538 cm^{-1} at the 15% NP concentration, means that until "this moment", exposed CH_2 groups for the higher NPs concentrations exist. The presence of both peaks indicates the optimum interfacial PVP-Nb area. For the concentrations 25–35%, where we can find the agglomeration effects, the CH_2 groups are "locked" inside the agglomerate, while the C–N and N–C=O groups are still interacting with the Nb_2O_5 surface.

The peak originating from the C=O group (1656) decreases with the NP concentration, and the intensity of the C-H peaks (2850–2952) noticeably increases with the NP concentration. These results clearly confirm the formation of C=O..HO-Nb groups. The formation of such bonds partially limits the rotational vibrations of the C=O group. The more that these groups are involved, the NPs partially organize the polymer chains, simultaneously stiffening the entire matrix. As a result of the partial ordering, a large number of dipoles forming the C-H groups align in parallel, resulting in a stronger signal in the infrared spectrum due to their combined dipole moment. The bands originating from the C-H groups remain strong at a concentration of 35%, while the sample's hydrophobicity decreases. This indicates that despite the chains being ordered at the molecular level, the macroscopic surface becomes more inorganic and dominated by Nb_2O_5, which reduces the composite's hydrophobic properties, which is what was confirmed in further contact angle analyses.

3.5. Microscopic and Contact Angle Analyses

The pieces of the same PVP and its composites with Nb_2O_5 samples were tested using SEM. Figure 9a–e presents morphology images at magnifications of 400× (a–b) and 1000× (c–e). Nb_2O_5 nanoparticles are visible on the surface of the images as bright spots. Figure 9a shows the surface of a pure PVP matrix without the addition of nanoparticles, and Figure 9b presents the morphology of the PVP film with a 5% Nb_2O_5 content. A few nanoparticle agglomerates are visible in the field of view. Figure 9c–e, which correspond to concentrations of 15, 25, and 35% Nb_2O_5 content, show larger and more numerous nanoparticle agglomerates. Based on the obtained results, we can conclude that the PVP/Nb_2O_5 films reveal significant morphological changes compared to the materials with a lower NPs concentration. The polymer matrix shows pronounced heterogeneity, and the presence of numerous highly contrasting bright regions indicates well-dispersed Nb_2O_5 nanoparticles. The higher content of the inorganic phase promotes the formation of particle clusters, suggesting progressive agglomeration. The increased number and size of the bright regions reflect the intensified influence of Nb_2O_5 on the composite's microstructure. SEM images of the Nb_2O_5 cluster, with the diameter marked, are shown in Supplementary Materials in Figure S4c.

The obtained contact angle measurement results (Figure 10) are consistent with the previously obtained results. In Figure 10a–d, the hydrophobicity of the films increases with the NPs concentration. In the case of the pure PVP film, the surface is smooth and moderately hydrophilic. For a concentration of 5% of Nb_2O_5, the hydrophilicity decreases slightly, with the appearance of isolated nanoparticle clusters when compared to the pure material. Hydrophobicity increases gradually up to a concentration of 25% and then decreases sharply when it reaches 35% (Figure 10e). This phenomenon can be explained by the supersaturation of the polymer matrix with the higher concentration of Nb_2O_5 NPs.

Larger and more numerous agglomerates are formed; thus, the sample surface becomes more textured, leading to a greater exposure of hydrophilic Nb_2O_5 regions. Furthermore, the increased number of nanoparticle aggregates enhances the film's porosity and capillarity, which, in turn, raises the overall hydrophilicity of the sample.

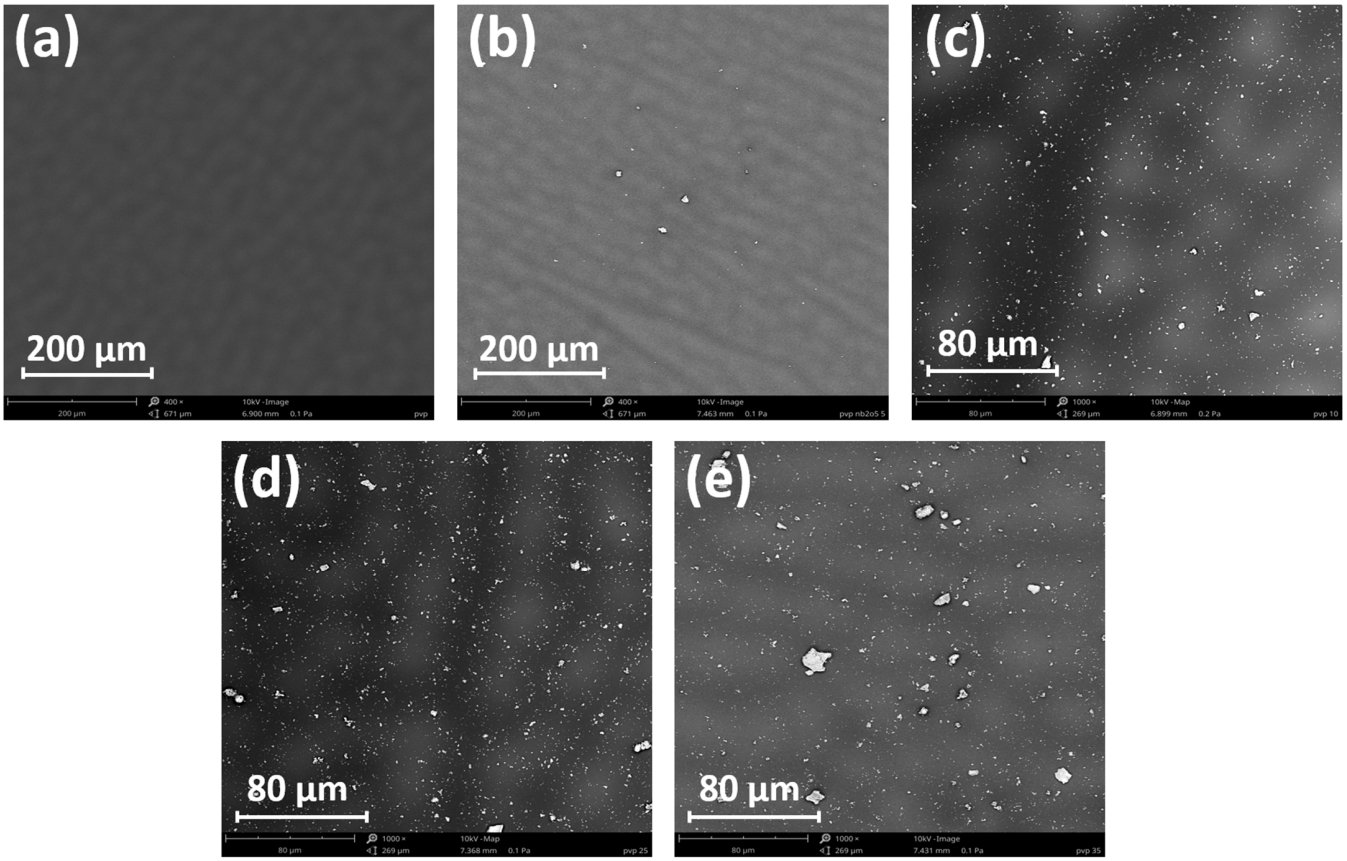


Figure 9. SEM pictures of the morphology of PVP (**a**) and its Nb_2O_5 composites at concentrations of 5% (**b**), 15% (**c**), 25% (**d**), and 35% (**e**).

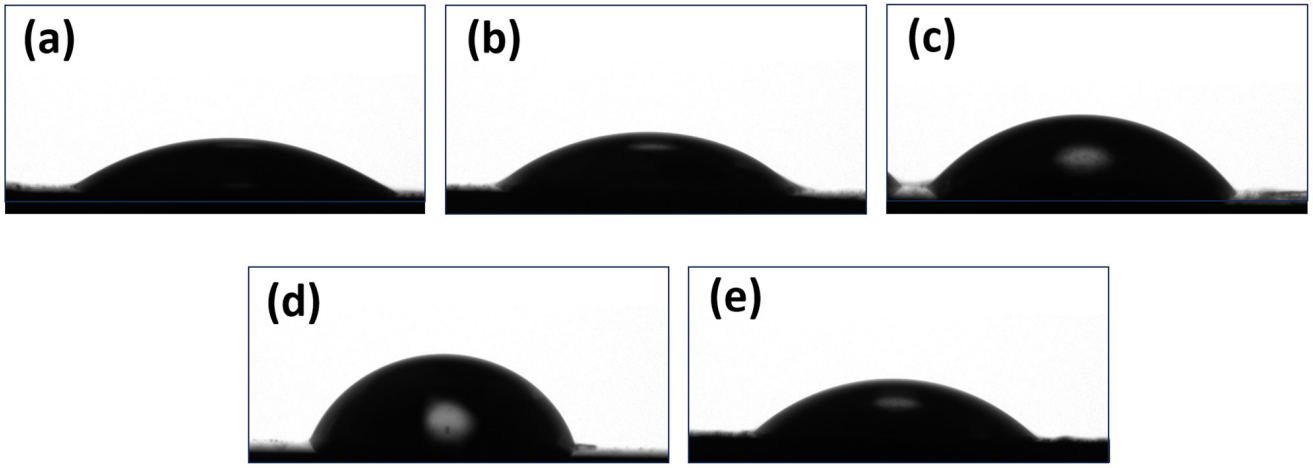


Figure 10. Measurements of the contact angle of PVP (**a**) and its Nb_2O_5 composites at concentrations of 5% (**b**), 15% (**c**), 25% (**d**), and 35% (**e**).

4. Conclusions

In this paper, we investigated PVP and its composites with Nb_2O_5 nanoparticle thin films. This study focused on comparing the physical properties of the samples with varying nanoparticle concentrations.

XRD analysis has confirmed the amorphous structure of the PVP matrix and the presence of Nb_2O_5 NPs in the polymer matrix, which was also confirmed using EDS analysis.

The transmission spectra revealed an increased UV absorption in the 320–700 nm range, with a higher nanoparticle content associated with a greater reduction in optical transmittance in this region, while the remainder of the spectra range remained transparent. According to the VASE experiments, the active contribution to the changes in the *n* dispersion was minimal (1.521–1.531 at λ = 2000 nm). The low values of the volume fraction coefficient clearly indicate that only a small proportion of Nb_2O_5 NPs actively contribute to the refractive index, confirming the presence of particles and agglomerates on the surface of the composite. The thermal analyses (DSC and VTSE) clearly showed the presence of two glass transition temperatures, both in pure PVP and in its composites. In the case of powdered material, T_{g1} remained constant and originated from the pyrrolidone moiety, and a variable T_{g2} was attributed to nanoparticle-induced stiffening of the polymer chains. The VTSE studies revealed an additional glass transition temperature (T_{gV2}), indicating the formation of an interfacial region between the PVP matrix and Nb_2O_5 nanoparticles due to hydrogen bonding at their interface. Due to the varying number of such bonds, we associate the changes in the T_{g2} temperature with an increase in Nb_2O_5 agglomerations. These results were confirmed by ATR-FTIR analysis, which clearly indicated the formation of C=O..HO-Nb groups. The SEM results revealed a homogeneous distribution of nanoparticles within the matrix, as well as an increase in the number and size of agglomerates. The contact angle measurements suggest that the most suitable concentrations appear to be 15% and 25%, at which the composite becomes relatively hydrophobic.

The results of this study demonstrate that the investigated PVP/Nb_2O_5 composites can be employed as prospective coatings to protect surfaces from UV radiation while maintaining the coating's relative hydrophobicity.

Supplementary Materials: The following supporting information can be downloaded at: https://www.mdpi.com/article/10.3390/polym17212939/s1, Figure S1: XRD pattern of Nb2O5 nanoparticles (a), pattern of PVP: Nb2O5 composite, with subtracted amorphous PVP hump (b), Figure S2: Non-normalised transmission spectra, Figure S3: FTIR spectrum of PVP (a), FTIR spectrum of PVP: Nb_2O_5 (5%) (b), FTIR spectrum of PVP: Nb_2O_5 (15%) (c), FTIR spectrum of PVP: Nb_2O_5 (25%) (d), FTIR spectrum of PVP: Nb_2O_5 (35%) (e), Figure S4: PVP EDS analysis (a), PVP: Nb_2O_5 EDS analysis (b), 7000× zoom on Nb_2O_5 cluster (c), Figure S5: SEM roughness 3D and 2D profile of PVP (a), SEM roughness 3D and 2D profile of PVP: Nb_2O_5 (5%) (b), SEM roughness 3D and 2D profile of PVP: Nb_2O_5 (15%) (c), SEM roughness 3D and 2D profile of PVP: Nb_2O_5 (25%) (d), SEM roughness 3D and 2D profile of PVP: Nb_2O_5 (35%) (e), Cut out of PVP: Nb_2O_5 map (f), Tables S1 and S2: EDS spot of PVP, Table S3: EDS spot of Nb_2O_5, Table S4: Results of roughness SEM analysis.

Author Contributions: Conceptualization, B.H., P.J. and M.M.; methodology, B.H. and P.J.; validation, B.H. and P.J.; formal analysis, B.H. and P.J.; investigation, B.H., P.J., P.K., M.G., M.B., S.K., M.Ł., M.M.S. and Ł.H.; data curation, B.H. and P.J.; writing—original draft preparation, B.H. and P.J.; writing—review and editing, B.H. and P.J.; visualization, B.H., P.J. and Ł.H.; supervision, B.H. and M.M. All authors have read and agreed to the published version of the manuscript.

Funding: This research received no external funding.

Institutional Review Board Statement: Not applicable.

Data Availability Statement: The original contributions presented in this study are included in the article. Further inquiries can be directed to the corresponding authors.

Conflicts of Interest: The authors declare no conflicts of interest.

References

1. Manias, E. The full potential of nanoparticles in imparting new functionalities in polymer nanocomposites remains largely untapped. A widely applicable, two-solvent processing approach provides a hierarchical structure, affording unparalleled composite performance enhancement. Nanocomposites: Stiffer by design. *Nat. Mater.* **2007**, *6*, 9–11. [CrossRef] [PubMed]
2. Yeh, J.M.; Liou, S.J.; Lin, C.Y.; Cheng, C.Y.; Chang, Y.W.; Lee, K.R. Anticorrosively Enhanced PMMA−Clay Nanocomposite Materials with Quaternary Alkylphosphonium Salt as an Intercalating Agent. *Chem. Mater.* **2002**, *14*, 154–161. [CrossRef]
3. Mathai, S.; Shaji, P.S. Polymer-Based Nanocomposite Coating Methods: A Review. *J. Sci. Res.* **2022**, *14*, 973–1002. [CrossRef]
4. Bhat, A.; Budholiya, S.; Raj, S.A.; Sultan, M.; Hui, D.; Shah, A.M.; Safri, S. Review on nanocomposites based on aerospace applications. *Nanotechnol. Rev.* **2021**, *10*, 237–253. [CrossRef]
5. Rahman, M.M.; Khan, K.H.; Parvez, M.M.H.; Irizarry, N.; Uddin, M.N. Polymer Nanocomposites with Optimized Nanoparticle Dispersion and Enhanced Functionalities for Industrial Applications. *Processes* **2025**, *13*, 994. [CrossRef]
6. Sazali, N.B.; Chan, L.W.; Wong, T.W. Nano-enabled agglomerates and compact: Design aspects of challenges. *Asian J. Pharm. Sci.* **2023**, *18*, 100794. [CrossRef]
7. Silva, M.R.F.; Alves, M.F.R.P.; Cunha, J.P.G.Q.; Costa, J.L.; Silva, C.A.; Fernandes, M.H.V.; Vilarinho, P.M.; Ferreira, P. Nanostructured transparent solutions for UV-shielding: Recent developments and future challenges. *Mat. Today Phys.* **2023**, *35*, 101131. [CrossRef]
8. Li, S.; Lin, M.M.; Toprak, M.S.; Kim, D.K.; Muhammed, M. Nanocomposites of polymer and inorganic nanoparticles for optical and magnetic applications. *Nano Rev.* **2010**, *1*, 5214. [CrossRef]
9. Blanchard, V.; Blanchet, P. Color stability for wood products during use: Effects of inorganic nanoparticles. *BioResources* **2011**, *6*, 1219–1229. [CrossRef]
10. Oladele, I.O.; Victor, O.O.; Omotosho, T.F.; Adebanjo, M.B.; Ayanleye, O.T.; Adekola, S.A. Sustainable polymer and polymer-based composite materials for extreme conditions and demanding applications—A review on pushing boundaries in materials science. *Next Mater.* **2025**, *8*, 100775. [CrossRef]
11. Gore, A.H.; Prajapat, A.L. Biopolymer Nanocomposites for Sustainable UV Protective Packaging. *Front. Mater.* **2022**, *9*, 855727. [CrossRef]
12. Khairy, Y.; Mohammed, M.I.; Elsaeedy, H.I.; Yahia, I.S. Optical and electrical properties of SnBr2-doped polyvinyl alcohol (PVA) polymeric solid electrolyte for electronic and optoelectronic applications. *Optik* **2021**, *228*, 166129. [CrossRef]
13. Ali, H.E.; Abdel-Aziz, M.; Ibrahiem, A.M.; Sayed, M.A.; Abd-Rabboh, H.S.M.; Awwad, N.S.; Algarni, H.; Shkir, M.; Khairy, M.Y. Microstructure Study and Linear/Nonlinear Optical Performance of Bi-Embedded PVP/PVA Films for Optoelectronic and Optical Cut-Off Applications. *Polymers* **2022**, *14*, 1741. [CrossRef]
14. Badawi, A. Engineering the optical properties of PVA/PVP polymeric blend in situ using tin sulfide for optoelectronics. *Appl. Phys. A Mater. Sci. Process.* **2020**, *126*, 335. [CrossRef]
15. Louie, S.M.; Gorham, J.M.; Tana, J.; Hackley, V.A. Ultraviolet photo-oxidation of polyvinylpyrrolidone (PVP) coatings on gold nanoparticles. *Environ. Sci. Nano* **2017**, *4*, 1866–1875. [CrossRef]
16. Hwang, J.M.; Kim, N.Y.; Shin, S.; Lee, J.H.; Ryu, J.Y.; Eom, T.; Park, B.K.; Kim, C.G.; Chung, T.-M. Synthesis of novel volatile niobium precursors containing carboxamide for Nb2O5 thin films. *Polyhedron* **2021**, *200*, 115134. [CrossRef]
17. Basuvalingam, S.B.; Macco, B.; Knoops, H.C.M.; Melskens, J.; Kessels, W.M.M.; Bol, A.A. Comparison of thermal and plasma-enhanced atomic layer deposition of niobium oxide thin films. *J. Vac. Sci. Technol. A* **2018**, *36*, 041503. [CrossRef]
18. Sousa Pereira, M.; Lima, A.; Almeida, R.; Martins, J.; Bagnis, D.; Barros, E.; Sombra, A.; Vasconcelos, I. Flexible, large-area organic solar cells with improved performance through incorporation of $CoFe_2O_4$ nanoparticles in the active layer. *Mater. Res.* **2019**, *22*, e20180640. [CrossRef]
19. Wang, T.-C.; Su, Y.-H.; Hung, Y.-K.; Yeh, C.-S.; Huang, L.-W.; Gomulya, W.; Lai, L.-H.; Loi, M.A.; Yang, J.-S.; Wu, J.-J. Charge collection enhancement by incorporation of gold–silica core–shell nanoparticles into P3HT:PCBM/ZnO nanorod array hybrid solar cells. *Phys. Chem. Chem. Phys.* **2015**, *17*, 19854–19861. [CrossRef]
20. Lu, Y.-M.; Chiang, C.-H.; Hsu, S.L.-C. The performance of polymer solar cells based on P3HT: PCBM after post-annealing and adding titanium dioxide nanoparticles. *Mater. Res. Innov.* **2014**, *18*, 102–105. [CrossRef]
21. Aleshin, A.N. Organic optoelectronics based on polymer—Inorganic nanoparticle composite materials. *Phys. Usp.* **2013**, *56*, 667–674. [CrossRef]
22. Asih, G.I.N.; Rafryanto, A.F.; Hartati, S.; Jiang, X.; Anggraini, A.; Yudhowijoyo, A.; Jiang, J.; Arramel. Recent advances of polymer nanocomposites in emerging applications. *Compos. Funct. Mater.* **2025**, *1*, 20250105–20250131. [CrossRef]

23. Singh, N.B.; Agarwal, S. Nanocomposites: An overview. *Emerg. Mater. Res.* **2016**, *5*, 5–43. [CrossRef]
24. Song, J.E.; Phenrat, T.; Marinakos, S.; Xiao, Y.; Liu, J.; Wiesner, M.R.; Tilton, R.D.; Lowry, G.V. Hydrophobic interactions increase attachment of gum arabic- and PVP-coated Ag nanoparticles to hydrophobic surfaces. *Environ. Sci. Technol.* **2011**, *45*, 5988–5995. [CrossRef]
25. Jebali, S.; Vayer, M.; Belal, K.; Sinturel, C. Engineered nanocomposite coatings: From water-soluble polymer to advanced hydrophobic performances. *Materials* **2024**, *17*, 574. [CrossRef]
26. Yousef, E.; Ali, M.K.M.; Allam, N.K. Tuning the optical properties and hydrophobicity of $BiVO_4$/PVC/PVP composites as potential candidates for optoelectronics applications. *Opt. Mater.* **2024**, *150*, 115193. [CrossRef]
27. Haaf, F.; Sanner, A.; Straub, F. Polymers of N-vinylpyrrolidone: Synthesis, characterization and uses. *Polym. J.* **1985**, *17*, 143–152. [CrossRef]
28. Kurakula, M.; Rao, G.S.N.K. Pharmaceutical assessment of polyvinylpyrrolidone (PVP): As excipient from conventional to controlled delivery systems with a spotlight on COVID-19 inhibition. *J. Drug Deliv. Sci. Technol.* **2020**, *60*, 102046. [CrossRef]
29. Khalid, M.U.; Rudokaite, A.; da Silva, A.M.H.; Kirsnyte-Snioke, M.; Stirke, A.; Melo, W.C.M.A. A comprehensive review of niobium nanoparticles: Synthesis, characterization, applications in health sciences, and future challenges. *Nanomaterials* **2025**, *15*, 106. [CrossRef]
30. Lopes, O.F.; Paris, E.C.; Ribeiro, C. Synthesis of Nb_2O_5 nanoparticles through the oxidant peroxide method applied to organic pollutant photodegradation: A mechanistic study. *Appl. Catal. B Environ.* **2014**, *144*, 800–808. [CrossRef]
31. Hajduk, B.; Bednarski, H.; Jarząbek, B.; Janeczek, H.; Nitschke, P. P3HT:PCBM blend films phase diagram on the base of variable-temperature spectroscopic ellipsometry. *Beilstein J. Nanotechnol.* **2018**, *9*, 1108–1115. [CrossRef] [PubMed]
32. Hajduk, B.; Bednarski, H.; Jarząbek, B.; Nitschke, P.; Janeczek, H. Phase diagram of P3HT:PC_{70}BM thin films based on variable-temperature spectroscopic ellipsometry. *Polym. Test.* **2020**, *84*, 106383. [CrossRef]
33. Hajduk, B.; Bednarski, H.; Jarka, P.; Janeczek, H.; Godzierz, M.; Tański, T. Thermal and optical properties of PMMA films reinforced with Nb_2O_5 nanoparticles. *Sci. Rep.* **2021**, *11*, 22531. [CrossRef]
34. Hajduk, B.; Jarka, P.; Tański, T.; Bednarski, H.; Janeczek, H.; Gnida, P.; Fijalkowski, M. An investigation of the thermal transitions and physical properties of semiconducting PDPP4T:PDBPyBT blend films. *Materials* **2022**, *15*, 8392. [CrossRef]
35. Hajduk, B.; Bednarski, H.; Domański, M.; Jarząbek, B.; Trzebicka, B. Thermal transitions in P3HT: PC_{60}BM films based on electrical resistance measurements. *Polymers* **2020**, *12*, 1458. [CrossRef]
36. Richter, U. *SpectraRay/3 Software Manual*; Sentech Instruments GmbH: Berlin, Germany, 2011.
37. Stoumbou, E.; Stavrakas, I.; Hloupis, G.; Alexandridis, A.; Triantis, D.; Moutzouris, K. A comparative study on the use of the extended-Cauchy dispersion equation for fitting refractive index data in crystals. *Opt. Quantum Electron.* **2013**, *45*, 837–859. [CrossRef]
38. Johnson, D.I.; Gadd, G.E.; Town, G.E. Total differential optical properties of polymer nanocomposite materials. In Proceedings of the 2006 International Conference on Nanoscience and Nanotechnology, ICONN 2006, Brisbane, Australia, 3–7 July 2006; IEEE: Piscataway, NJ, USA, 2006; pp. 423–426. [CrossRef]
39. Buera, M.D.P.; Levi, G.; Karel, M. Glass transition in poly(vinylpyrrolidone): Effect of molecular weight and diluents. *Biotechnol. Prog.* **1992**, *8*, 144–148. [CrossRef]
40. Maidannyk, V.A.; Mishra, V.S.N.; Miao, S.; Djali, M.; McCarthy, N.; Nurhadi, B. The effect of polyvinylpyrrolidone addition on microstructure, surface aspects, the glass transition temperature and structural strength of honey and coconut sugar powders. *J. Future Foods* **2022**, *2*, 338–345. [CrossRef]
41. Gatica, N.; Soto, L.; Moraga, C.; Vergara, L. Blends of poly(N-vinyl-2-pyrrolidone) and dihydric phenols: Thermal and infrared spectroscopic studies. Part IV. *J. Chil. Chem. Soc.* **2013**, *58*, 1978–1983. [CrossRef]
42. Restrepo, I.; Velásquez, E.; Galotto, M.; Guarda, A. Influence of the molar mass and concentration of polyvinylpyrrolidone on the physical–mechanical properties of polylactic acid for food packaging. *Polymers* **2025**, *17*, 2218. [CrossRef]
43. Vyazovkin, S.; Dranca, I. Probing beta relaxation in pharmaceutically relevant glasses by using DSC. *Pharm. Res.* **2006**, *23*, 422–428. [CrossRef] [PubMed]
44. Fox, T.G.; Flory, P.J. The glass temperature and related properties of polystyrene. Influence of molecular weight. *J. Polym. Sci.* **1954**, *14*, 315–319. [CrossRef]
45. Jarka, P.; Hajduk, B.; Kumari, P.; Janeczek, H.; Godzierz, M.; Tsekpo, Y.M.; Tański, T. Investigations on thermal transitions in PDPP4T/PCPDTBT/AuNPs composite films using variable temperature ellipsometry. *Polymers* **2025**, *17*, 704. [CrossRef] [PubMed]
46. Hajduk, B.; Jarka, P.; Bednarski, H.; Godzierz, M.; Tański, T.; Staszuk, M.; Nitschke, P.; Jarząbek, B.; Fijalkowski, M.; Mazik, K. Thermal and optical properties of P3HT:PC70BM: ZnO nanoparticles composite films. *Sci. Rep.* **2024**, *14*, 66. [CrossRef]
47. White, R.P.; Lipson, J.E.G.; Keddie, J.L. Spectroscopic ellipsometry as a route to thermodynamic characterization. *Soft Matter* **2022**, *18*, 6660–6673. [CrossRef]

48. Wang, T.; Hu, S.; Zhang, S.; Peera, A.; Reffner, J.; Torkelson, J.M. Eliminating the Tg-Confinement Effect in Polystyrene Films: Extraordinary Impact of a 2 mol % 2-Ethylhexyl Acrylate Comonomer. *Macromolecules* **2022**, *55*, 9601–9611. [CrossRef]
49. Serna, S.; Wang, T.; Torkelson, J.M. Eliminating the Tg-confinement and fragility-confinement effects in poly(4-methylstyrene) films by incorporation of 3 mol % 2-ethylhexyl acrylate comonomer. *J. Chem. Phys.* **2024**, *160*, 034903. [CrossRef]
50. Ali, H.E.; Sayed, M.A.; Algarni, H.; Khairy, Y.; Abdel-Aziz, M.M. Use of niobium oxide nanoparticles as nanofillers in PVP/PVA blends to enhance UV–visible absorption, opto-linear, and nonlinear optical properties. *J. Vinyl Addit. Technol.* **2022**, *28*, 444–452. [CrossRef]

Disclaimer/Publisher's Note: The statements, opinions and data contained in all publications are solely those of the individual author(s) and contributor(s) and not of MDPI and/or the editor(s). MDPI and/or the editor(s) disclaim responsibility for any injury to people or property resulting from any ideas, methods, instructions or products referred to in the content.